How abundant are superoxide and hydrogen peroxide in the vasculature lumen, how far can they reach?

Tânia Sousa [a,b,c], Marcos Gouveia [c], Rui D.M. Travasso [c,*], Armindo Salvador [a,d,e,**]

[a] *CNC – Centre for Neuroscience Cell Biology, University of Coimbra, UC-Biotech, Parque Tecnológico de Cantanhede, Núcleo 4, Lote 8, 3060-197, Cantanhede, Portugal*
[b] *Faculty of Science and Technology, Rua Sílvio Lima, Universidade de Coimbra – Polo II, 3030-790, Coimbra, Portugal*
[c] *CFisUC, Department of Physics, University of Coimbra, Rua Larga, 3004-516, Coimbra, Portugal*
[d] *Coimbra Chemistry Center - Institute of Molecular Sciences (CQC-IMS), University of Coimbra, Rua Larga, 3004-535, Coimbra, Portugal*
[e] *Institute for Interdisciplinary Research, University of Coimbra, Casa Costa Alemão, Rua Dom Francisco de Lemos, 3030-789, Coimbra, Portugal*

ARTICLE INFO

ABSTRACT

Paracrine superoxide ($O_2^{\bullet-}$) and hydrogen peroxide (H_2O_2) signaling critically depends on these substances' concentrations, half-lives and transport ranges in extracellular media. Here we estimated these parameters for the lumen of human capillaries, arterioles and arteries using reaction-diffusion-advection models. These models considered $O_2^{\bullet-}$ and H_2O_2 production by endothelial cells and uptake by erythrocytes and endothelial cells, $O_2^{\bullet-}$ dismutation, $O_2^{\bullet-}$ and H_2O_2 diffusion and advection by the blood flow. Results show that in this environment $O_2^{\bullet-}$ and H_2O_2 have half-lives <60. ms and <40. ms, respectively, the former determined by the plasma SOD3 activity, the latter by clearance by endothelial cells and erythrocytes. H_2O_2 concentrations do not exceed the 10 nM scale. Maximal $O_2^{\bullet-}$ concentrations near vessel walls exceed H_2O_2's several-fold when the latter results solely from $O_2^{\bullet-}$ dismutation. Cytosolic dismutation of inflowing $O_2^{\bullet-}$ may thus significantly contribute to H_2O_2 delivery to cells. $O_2^{\bullet-}$ concentrations near vessel walls decay to 50% of maximum 12 μm downstream from $O_2^{\bullet-}$ production sites. H_2O_2 concentrations in capillaries decay to 50% of maximum 22 μm (6.0 μm) downstream from $O_2^{\bullet-}$ (H_2O_2) production sites. Near arterioles' (arteries') walls, they decay by 50% within 6.0 μm (4. μm) of H_2O_2 production sites. However, they reach maximal values 50 μm (24 μm) downstream from $O_2^{\bullet-}$ production sites and decrease by 50% over 650 μm (500 μm). Arterial/olar endothelial cells might thus signal over a mm downstream through $O_2^{\bullet-}$-derived H_2O_2, though this requires nM-sensitive H_2O_2 transduction mechanisms.

1. Introduction

Signaling through superoxide ($O_2^{\bullet-}$) and hydrogen peroxide (H_2O_2) released by cells to the extracellular medium mediates numerous physiological processes [1–6]. However, whether such signaling is autocrine, near-cell paracrine or volume is under discussion [7–10]. Likewise, the extracellular concentrations involved in physiological signaling remain uncertain, and this knowledge is critical to understand what intracellular mechanisms can viably transduce such signals [11, 12].

Redox signaling plays a prominent role in vascular processes [4,5, 13–16]. For example, H_2O_2 may act as an agent that promotes endothelial derived hyperpolarization of vascular endothelial and smooth muscle cells by stimulating the elevation of the concentration of Ca^{2+} ions and opening of K_{Ca} channels. This increase in cell polarization is associated to vascular dilation [17]. The present work focuses on signaling through the microvasculature lumen, where the blood flow may help $O_2^{\bullet-}$ and H_2O_2 reach downstream cells. Mechanical and other types of stimuli to vascular endothelial cells (EC) trigger intracellular phosphorylation cascades that activate NADPH oxidase 2 (NOX2) at the plasma membrane [4]. NOX2 catalyzes one-electron O_2 reduction by cytosolic NADPH at a 2 O_2/NADPH stoichiometry. The resulting $O_2^{\bullet-}$ is released to the extracellular medium, where it has three main fates. First, it is absorbed by both erythrocytes and ECs through chloride channels [18–20], and then dismutated to O_2 and H_2O_2 via cytosolic superoxide dismutase (SOD1). Second, it is dismutated via extracellular superoxide dismutase (SOD3). Erythrocytes and ECs absorb the resulting H_2O_2 [21,22], which readily oxidizes the cytosolic peroxiredoxins (Prdx) 1 and 2 ($k = 0.13$-1.6×10^8 $M^{-1}s^{-1}$ [23–26]), eventually driving

---

Abbreviations:

BAEC	bovine artery endothelial cells
EC	endothelial cell
NOX	NADPH oxidase
Prdx	peroxiredoxin
SOD	superoxide dismutase

redox relays that transduce these signals [27–30]. Third, it reacts extremely fast with nitric oxide ($^\bullet$NO) ($k = 1.9 \times 10^{10}$ M^{-1}s^{-1} [31,32]). Consequently, in the presence of typical nM $^\bullet$NO concentrations in blood plasma [33], $O_2^{\bullet-}$ has a half-life <30 ms. The resulting peroxynitrite (ONOO$^-$) [34] can also cross cell membranes through anion channels and by passive permeation [35–37], and quickly oxidizes Prdx1/2 ($k \approx 10^7$ M^{-1}s^{-1} [25,38]). However, most of it reacts with CO_2 (1.3 mM in plasma, $k = 5.8 \times 10^4$ M^{-1}s^{-1} [32,39]) and other blood plasma components. Therefore, $^\bullet$NO production by the ECs suppresses $O_2^{\bullet-}$-derived H_2O_2 production, and the ONOO$^-$ thus formed cannot functionally replace H_2O_2 in redox signaling. To a good approximation, only the excess $O_2^{\bullet-}$ production over the $^\bullet$NO production is available for H_2O_2-mediated signaling. Contractile vessels continuously produce $^\bullet$NO to maintain their vascular tone, which should eliminate most of the $O_2^{\bullet-}$. However, in the early moments after a stimulus that increased $O_2^{\bullet-}$ production or/and decreased $^\bullet$NO production, before the vasoconstriction response, an excess $O_2^{\bullet-}$ production can coexist with laminar flow.

Whether ECs can also directly release H_2O_2 to the vascular lumen remains contentious [15,40]. ECs abundantly express NOX4 [15,40], which catalyzes O_2 reduction to H_2O_2 by NADPH at a rate that is sensitive to physiological O_2 concentrations [41]. However, most of the NOX4 in ECs localizes to internal membranes, and evidence that some of it localizes to the cell membrane is lacking [40]. Nevertheless, there is evidence that NOX4 levels modulate H_2O_2 release by murine lung ECs and by the intact mouse aorta [15], and therefore the possibility that ECs release H_2O_2 to the vascular lumen deserves consideration.

Mathematical modeling has previously proved informative about the spatial distribution and dynamics of reactive nitrogen/oxygen species in the vasculature (eg. Refs. [42–48]). Therefore, here we used reaction-diffusion-advection models to estimate how far $O_2^{\bullet-}$ and H_2O_2 can travel through capillaries, arterioles and arteries, and what concentrations are attainable under conditions where ECs release $O_2^{\bullet-}$ in excess of $^\bullet$NO or release H_2O_2. We have also examined what are the main determinants of these distances and concentrations. We discuss these results in the context of other works that address the distribution, concentration and lifetimes of H_2O_2 in animal tissues.

2. Models, parameter estimates and methods

2.1. Models and methods

The implemented reaction-advection-diffusion models of the spatio-temporal dynamics of $O_2^{\bullet-}$ and H_2O_2 concentrations (C_O, and C_H, respectively) in the vasculature lumen consider the processes and geometries depicted in Fig. 1. In here, C_O and C_H depend on the position along the vessel, z, and on the distance r to the center of the vessel according to the following equations:

$$\frac{\partial C_O}{\partial t} = D_O \left(\frac{1}{r} \frac{\partial}{\partial r} \left(r \frac{\partial C_O}{\partial r} \right) + \frac{\partial^2 C_O}{\partial z^2} \right) - v(r) \frac{\partial C_O}{\partial z} - 2k_d C_O - k_{O,B} Hc(r) C_O \,,$$
(1)

$$\frac{\partial C_H}{\partial t} = D_H \left(\frac{1}{r} \frac{\partial}{\partial r} \left(r \frac{\partial C_H}{\partial r} \right) + \frac{\partial^2 C_H}{\partial z^2} \right) - v(r) \frac{\partial C_H}{\partial z} + k_d C_O - k_{H,B} Hc(r) C_H \,,$$
(2)

where the symbols have the meanings described in Table 1. We assume that blood is flowing in the laminar regime, with its velocity following Poiseuille's law, $v(r) = v_{max}(R^2 - r^2)$.

We consider that $O_2^{\bullet-}$ is released to the lumen by a 20 μm-long ring of ECs (the length of a large EC), which also intake $O_2^{\bullet-}$ and H_2O_2 as all the other ECs. This is achieved with the following boundary conditions at the vessel wall:

$$D_O \frac{\partial C_O}{\partial r} \bigg|_{r=R} = P \, \delta_c(z) - \kappa_{O,E} C_O(R,z),$$

$$D_H \frac{\partial C_H}{\partial r} \bigg|_{r=R} = - \kappa_{H,E} C_H(R,z),$$

where $\delta_c(z) = 1$ at the $O_2^{\bullet-}$-producing cells and $\delta_c(z) = 0$ everywhere else along the vessel wall.

In capillaries (Fig. 1A), erythrocytes accumulate in the vicinity of the vessel axis, leaving an erythrocyte-free zone near the vessel wall [59, 55]. Accordingly, in a neighborhood of width $\Delta = 1.65$ μm of the vessel wall the hematocrit is set to zero, and a "wall" of erythrocytes is located at $r = R - \Delta$. Here, we implement the following boundary conditions,
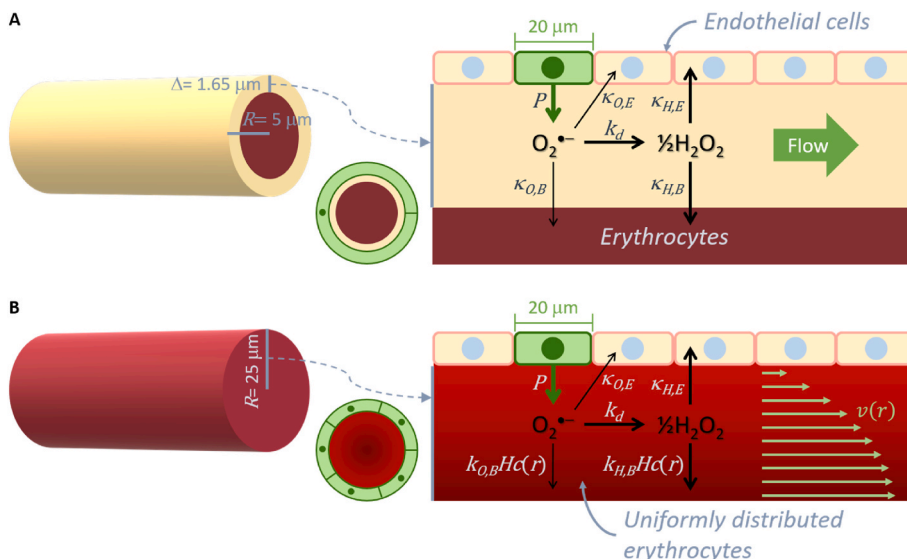
Fig. 1. Simulated processes and geometries for capillaries (A) and arterioles and arteries (B). (Right) Simulated processes: Superoxide release at the surface of an EC ring, $O_2^{\bullet-}$ dismutation, $O_2^{\bullet-}$ and H_2O_2 advection, $O_2^{\bullet-}$ and H_2O_2 uptake by the EC and erythrocyte layers in capillaries (A) or by the EC layer and uniformly dispersed erythrocytes in arterioles (B). (Left) Schematic diagram of the simulated capillary vessel (A) with an erythrocyte-free region at the vicinity of the vessel wall, similarly to experimental observations, and arteriole (B), with the hematocrit distributed throughout the vessel cross section. (Center) Cross-section of the vessels, showing the capillaries surrounded by one (A) and the arterioles by five (B) $O_2^{\bullet-}$-producing EC. For small arteries, the considered geometry was similar to that for arterioles, but with R = 150 μm and 30 surrounding ECs.

Table 1
Symbol meanings and parameter values.

Vessel	Symbol	Meaning	Value	References
All	P	Area-specific $O_2^{\bullet-}$ production rate of $O_2^{\bullet-}$-producing cells	6.0×10^2 molec. $s^{-1} \mu m^{-2}$	See text
	D_O	$O_2^{\bullet-}$ diffusion constant	$2.52 \times 10^3 \, \mu m^2 \, s^{-1}$	[49]
	D_H	H_2O_2 diffusion constant	$1.83 \times 10^3 \, \mu m^2 \, s^{-1}$	[50]
	k_d	$O_2^{\bullet-}$ dismutation pseudo-first-order rate constant in blood plasma	$9.3 \, s^{-1}$	[51]
	$\kappa_{H,E}$	Permeability constant of EC membranes for H_2O_2	$19. \, \mu m \, s^{-1}$	[21]
	$\kappa_{O,E}$	Permeability constant of EC membranes for $O_2^{\bullet-}$	$1.9 \, \mu m \, s^{-1}$	See text
	$\kappa_{H,B}$	Permeability constant of erythrocyte membranes for H_2O_2	$16. \, \mu m \, s^{-1}$	[22]
	$\kappa_{O,B}$	Permeability constant of erythrocyte membranes for $O_2^{\bullet-}$	$1.9 \, \mu m \, s^{-1}$	See text
	V_E	Erythrocyte volume	$97. \, \mu m^3$	[52]
	A_E	Erythrocyte surface area	$135. \, \mu m^2$	[52]
	$\overline{Hc}$	Mean hematocrit	0.45	[53]
Capillaries	R	Radius	$5.0 \, \mu m$	[54]
	Δ	Width of plasma region	$1.65 \, \mu m$	[55]
	v_{max}	Maximum velocity of blood flow	$5.0 \times 10^2 \, \mu m \, s^{-1}$	[56]
Arterioles	R	Radius	$25. \, \mu m$	[54]
	v_{max}	Maximum velocity of blood flow	$1.0 \times 10^4 \, \mu m \, s^{-1}$	[56]
	$k_{H,B}$	Effective rate constant for H_2O_2 consumption by erythrocytes	$18. \, s^{-1}$	$\frac{\kappa_{H,B} A_E}{V_E} \frac{\overline{Hc}}{1-\overline{Hc}}$
	$k_{O,B}$	Effective rate constant for $O_2^{\bullet-}$ consumption by erythrocytes	$2.2 \, s^{-1}$	$\frac{\kappa_{O,B} A_E}{V_E} \frac{\overline{Hc}}{1-\overline{Hc}}$
Small arteries	R	Radius	$150. \, \mu m$	[57]
	v_{max}	Maximum velocity of blood flow	$2.0 \times 10^5 \, \mu m \, s^{-1}$	[58]
	$k_{H,B}$	Effective rate constant for H_2O_2 consumption by erythrocytes	$18. \, s^{-1}$	As for arterioles
	$k_{O,B}$	Effective rate constant for $O_2^{\bullet-}$ consumption by erythrocytes	$2.2 \, s^{-1}$	As for arterioles

which describe the intake of $O_2^{\bullet-}$ and H_2O_2 by the erythrocytes:

$$D_O \frac{\partial C_O}{\partial r}\bigg|_{r=R-\Delta} = \kappa_{O,B} C_O(R,z),$$

$$D_H \frac{\partial C_H}{\partial r}\bigg|_{r=R-\Delta} = \kappa_{H,B} C_H(R,z).$$

In turn, for the arteriole (Fig. 1B), the hematocrit function, $Hc(r) = 1.045 \times \left(\frac{1}{1+e^{\left(\frac{10r}{25}-10\right)}} - 0.5 \right)$, where r is measured in μm, is fitted to observations reported in 1.4A of reference [55]. For the artery the same function for the hematocrit is used in the 125 μm $< r <$ 150 μm range, while for $0 < r < 125$ μm we consider a constant value for the hematocrit, $Hc(r) = 0.5225$. In both these cases, we implement Neumann boundary conditions at the center of the vessel:

$$\frac{\partial C_O}{\partial r}\bigg|_{r=0} = \frac{\partial C_H}{\partial r}\bigg|_{r=0} = 0.$$

Periodic boundary conditions on C_O and C_H are implemented at the extremities of the vessel ($z = 0$ and $z = z_{max}$). Nevertheless, the site of $O_2^{\bullet-}$-producing cells and the length of the simulation boxes are chosen such that both C_O and C_H are vanishingly small at both extremities.

Henceforth we will denote the just-described models for capillaries and arterioles/arteries by "Model C" and "Model A″", respectively.

The models for the case where ECs release H_2O_2 instead of $O_2^{\bullet-}$ are particular cases of the formulations above obtained by neglecting Equation (1) and the boundary conditions for $O_2^{\bullet-}$, by setting $k_d = 0$ in Equation (2), and by introducing the H_2O_2 production term $\frac{1}{2}P\delta_c(z)$ in the corresponding boundary condition. (Note that $O_2^{\bullet-}$ dismutation generates one H_2O_2 molecule from two $O_2^{\bullet-}$ ions, and consequently systems with $O_2^{\bullet-}$ production equal to P and with H_2O_2 production equal to $\frac{1}{2}P$ generate H_2O_2 at the same rate if all the $O_2^{\bullet-}$ is dismutated.)

Equations (1) and (2) were integrated numerically using finite differences in simulation boxes of sizes 33×200 for the capillary ($\Delta r = 0.05$ μm and $\Delta z = 2$ μm), 20×2500 for the arteriole ($\Delta r = 1.25$ μm and $\Delta z = 2$ μm), and 120×5000 for the artery ($\Delta r = 1.25$ μm and $\Delta z = 2$ μm). The integration was carried out until the concentrations reached their stationary values.

The same code, with $\delta_c(z) = 1$ throughout the vessel's length, was used to obtain C_O and C_H when all ECs produce either $O_2^{\bullet-}$ or H_2O_2.

2.2. Parameter estimates

2.2.1. Superoxide and hydrogen peroxide concentrations and production rates in the microvasculature

In this linear model, the spatial distributions of $O_2^{\bullet-}$ and H_2O_2 concentrations are independent of the $O_2^{\bullet-}$ or H_2O_2 release rate by human microvascular ECs, but knowing the value of this parameter is essential to estimate local $O_2^{\bullet-}$ and H_2O_2 concentrations. Because we are unaware of any experimental determinations of this rate, we assessed its plausible range based on the following findings. Cultured BAEC released $(0.64–1.9) \times 10^5$ H_2O_2 molecules/s/cell in the physiological range of tissue O_2 concentrations [60,61]. These authors did not determine whether the detected H_2O_2 resulted from dismutation of released $O_2^{\bullet-}$ or was directly released by the cells. Therefore, we analyzed two extreme scenarios. In the first scenario, which appears closer to reality, we assumed that all the detected H_2O_2 resulted from dismutation of released $O_2^{\bullet-}$ that escaped reaction with eventually produced $^{\bullet}NO$ and reabsorption by the cells. This translates into a $(1.2–3.8) \times 10^5$ $O_2^{\bullet-}$ molecules/s/cell *net* release rate. Dividing this range's upper bound by the area of contact of an EC with the vessel lumen in the considered geometry yields the reference value of P in Table 1. Despite species, cell type and environment differences, basal net $O_2^{\bullet-}$ release rates by human vascular ECs *in vivo* can reasonably be expected to be in the same order of magnitude. In turn, some cells release $O_2^{\bullet-}$ at much higher rates when

stimulated: 4×10^6 $O_2^{\bullet-}$ molecules/s/cell for internal mammary smooth muscle cells stimulated with 100 U/ml IL-1β [62], and $(1-40) \times 10^6$ $O_2^{\bullet-}$ molecules/s/cell for polymorphonuclear leukocytes and Kupffer cells [63,64]. In the second scenario we assumed that all the detected H_2O_2 was directly released.

2.2.2. Permeability of ECs and erythrocytes to $O_2^{\bullet-}$ and H_2O_2

Under physiological conditions, both $O_2^{\bullet-}$ and H_2O_2 are readily consumed in the cytosol of erythrocytes and ECs, the former species by superoxide dismutase and the latter by Prdx. Therefore, the rates of cellular consumption of these species in the blood plasma is limited by these cells' membrane permeabilities.

Orrico et al. [22] determined a 16. μm s^{-1} permeability constant of human erythrocytes for H_2O_2, 2.8-fold higher than a previous more indirect estimate [65]. We estimated a 19. μm s^{-1} permeability constant from H_2O_2 consumption rates determined in Ref. [21] for HUVEC cultures exposed to low H_2O_2 concentrations (details in Supplementary Information section 1, SI1).

Erythrocytes and ECs are permeable to $O_2^{\bullet-}$ [18–20], but we are unaware of experimental data to estimate the corresponding permeability constants. So, we considered the permeability constants of both erythrocyte and EC membranes for $O_2^{\bullet-}$ as 1/10th of that estimated for H_2O_2 in ECs and assessed the effect of changing this estimate.

3. Results

Below we focus mainly on EC-to-EC signaling, for which the $O_2^{\bullet-}$ and H_2O_2 concentrations at the ECs' surface and their influx rates are the most relevant considerations. The range over which cells can communicate through a diffusible substance depends on how far it is transported within its lifetime and on the concentration threshold for signaling. We will express the former parameter as the distance at which the $O_2^{\bullet-}$ and H_2O_2 concentrations decrease to 50% of maximum values. In turn the minimal thresholds for H_2O_2 signaling in EC are presently unclear. Shaji et al. [13] recently reported that treatment of Matrigel-seeded blood-brain barrier microvascular ECs with 1–10 nM H_2O_2 boluses for 2 h significantly increased EC tube length in a dose-dependent way. This observation suggests that ECs can sense and respond to H_2O_2 concentrations in the nM range. However, this inference needs confirmation by experiments including the determination of *in situ* H_2O_2 concentrations, as $O_2^{\bullet-}/H_2O_2$ release by the ECs themselves might lead to substantially higher local concentrations than the nominal ones. On the other hand, signaling likely requires local extracellular concentrations to substantially exceed cytosolic ones. This is because virtually all the signal transduction mechanisms for extracellular H_2O_2

considered to date depend on H_2O_2 influx into cells [11,66,67], and H_2O_2 is not known to be actively transported across membranes. As basal cytosolic H_2O_2 concentrations in human cells are in the 0.1 nM range [68,69], below we consider extracellular H_2O_2's concentration threshold for signaling as 1 nM.

3.1. Potential $O_2^{\bullet-}$ and H_2O_2 signaling in capillaries is short-range

Numerical integration of Model C reveals that the $O_2^{\bullet-}$ and H_2O_2 concentrations at the surface of the ECs are very localized at the vicinity of the $O_2^{\bullet-}$-producing cell (green cell in Fig. 2A). The concentrations of $O_2^{\bullet-}$ and H_2O_2 steeply decrease in the longitudinal direction away from the $O_2^{\bullet-}$ supply zone, reaching 50% of their maximal values within 12 μm and 22 μm downstream of the site where the peak concentration is reached, respectively. And the H_2O_2 concentration falls below the 1 nM signaling threshold within 46. μm of the peak. In turn, the concentrations of both species remain virtually constant in the radial direction over the short span of the plasma region (Fig. 2B and C). This region is so narrow that molecules of both species cross it within 1 ms, given their diffusion constants. The large contact areas of the plasma with the EC and erythrocyte layers and the narrow width of the plasma layer, lead to the rapid absorption of $O_2^{\bullet-}$ and H_2O_2 by both erythrocytes and ECs. The following fractions of $O_2^{\bullet-}$ and H_2O_2 that are absorbed by each layer or dismutated (in the case of $O_2^{\bullet-}$) at steady state for the reference parameter values in Table 1 can be readily calculated (SI2). Of the $O_2^{\bullet-}$ molecules, 80% are dismutated, while the other 12% are absorbed by the ECs and 8% are absorbed by erythrocytes. In turn, of the H_2O_2 molecules, 64% are absorbed by the ECs, while the other 36% are absorbed by the erythrocytes in the capillary.

The blood flow causes a slight asymmetry of concentration distributions around the $O_2^{\bullet-}$ supply zone, and a small 2 μm gap between the concentration peak of H_2O_2 and that of $O_2^{\bullet-}$, reflecting some $O_2^{\bullet-}$ advection before dismutation (Fig. 2A). But altogether, these results show that the slow blood flow in capillaries does not substantially advect $O_2^{\bullet-}$ and H_2O_2 during their short lifetime, their spread being diffusion-dominated.

3.2. Short-range $O_2^{\bullet-}$ and long-range H_2O_2 transport in arterioles and arteries

Numerical integration of Model A reveals a very different distribution of $O_2^{\bullet-}$ and H_2O_2 at the ECs' surface in arterioles (Fig. 3A). The $O_2^{\bullet-}$ concentration attains its maximum in the longitudinal direction within the supply zone (in green) and decays by 50% by 12 μm downstream. In contrast, the H_2O_2 concentration has a broad maximum, peaking at 50
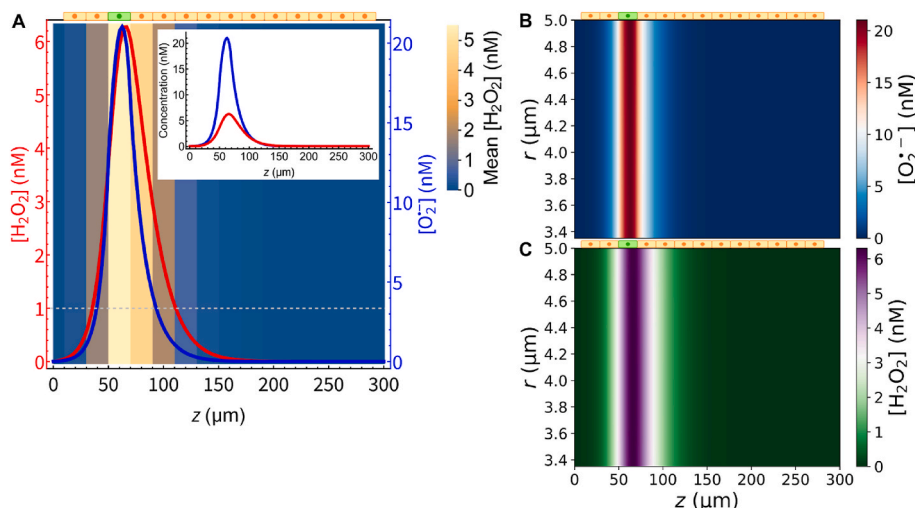
Fig. 2. Spatial distribution of $O_2^{\bullet-}$ and H_2O_2 in capillaries. (A) $O_2^{\bullet-}$ (blue) and H_2O_2 (red) concentrations at the surface of the ECs along the arteriole length. The background colors represent the average concentration at the surface of each EC represented at the top. The horizontal dashed line marks the assumed signaling threshold. The inset shows the H_2O_2 and $O_2^{\bullet-}$ concentrations in the same scale. (B,C) $O_2^{\bullet-}$ (B) and H_2O_2 (C) concentrations along the radial and longitudinal directions. The position of the $O_2^{\bullet-}$-producing ECs is marked in green in all panels. (For interpretation of the references to color in this figure legend, the reader is referred to the Web version of this article.)
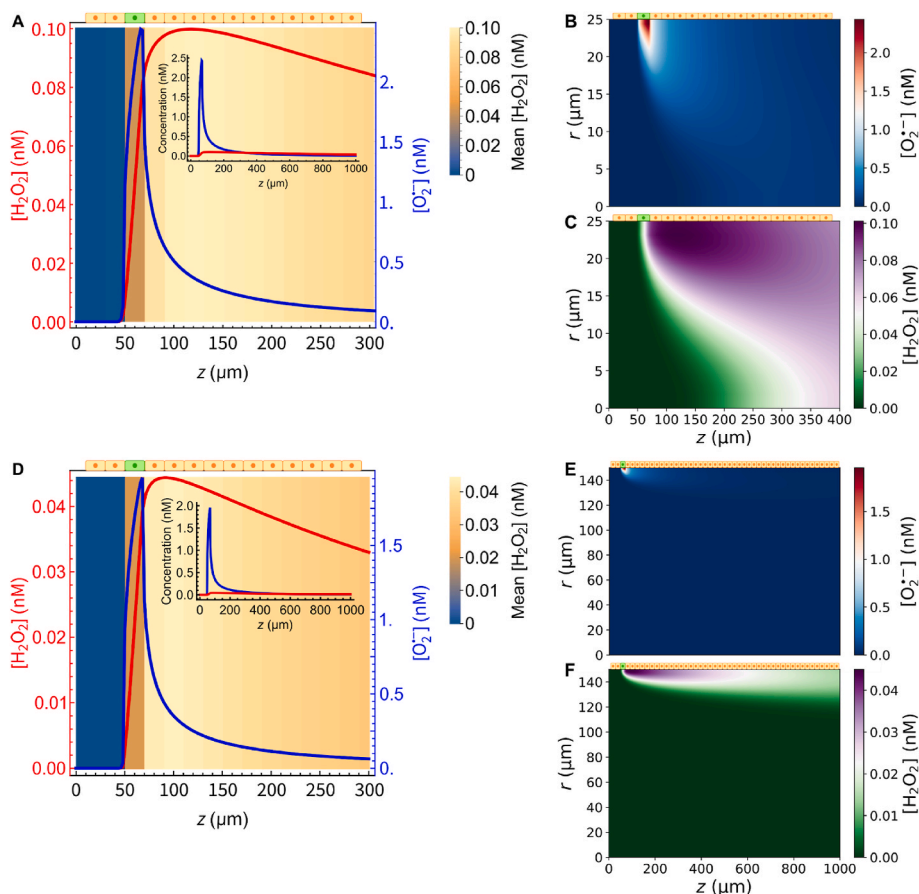
Fig. 3. Spatial distribution of $O_2^{\bullet-}$ and H_2O_2 in arterioles and arteries. (A,D) $O_2^{\bullet-}$ (blue) and H_2O_2 (red) concentrations at the surface of the ECs along the arteriole (A) and the artery (D) length. The background colors represent the average concentration at the surface of each EC represented at the top. The insets show the H_2O_2 and $O_2^{\bullet-}$ concentrations in the same scale over a longer segment of the 5 mm- and 1 cm-long simulated arteriole and artery, respectively. (B,C,E,F) H_2O_2 (B,E) and $O_2^{\bullet-}$ (C,F) concentrations along the radial and longitudinal directions in the arteriole (B,C) and in the artery (E,F). The position of the $O_2^{\bullet-}$-producing ECs is marked in green in all panels. Note the distinct length and concentration scales in (D–F) vs. (A–C). (For interpretation of the references to color in this figure legend, the reader is referred to the Web version of this article.)

μm downstream of the $O_2^{\bullet-}$ maximum, and decays by 50% over 650 μm downstream from the maximum. The concentrations of both species also decrease substantially in the radial direction away from the $O_2^{\bullet-}$-producing ECs (Fig. 3B and C), with H_2O_2 penetrating deeper into the vessel.

The very different distribution of $O_2^{\bullet-}$ and H_2O_2 at the ECs' surface has the following explanation. Because the velocity of blood near the vessel's wall is very low, $O_2^{\bullet-}$ molecules that stay in this region are not significantly advected down the arteriole before being dismutated or uptaken. $O_2^{\bullet-}$ molecules that diffuse deeper into the arteriole are further advected by the faster blood flow therein, those returning to near the ECs' surface explaining the long tail of the $O_2^{\bullet-}$ concentration profile in Fig. 3A. However, most of that $O_2^{\bullet-}$ dismutates and yields H_2O_2 well inside the arteriole's lumen. From there, the blood flow substantially advects H_2O_2 while it diffuses back to the ECs' surface. This causes the 50 μm gap between the concentration peaks of H_2O_2 and $O_2^{\bullet-}$, and the shallowness of the longitudinal decline of the H_2O_2 concentration.

The predominant fates of $O_2^{\bullet-}$ and H_2O_2 in arterioles also differ substantially from those in capillaries. Of the $O_2^{\bullet-}$ molecules, 95% are dismutated, while the other 5% are absorbed by the ECs and erythrocytes. In turn, of the H_2O_2 molecules, 18% are absorbed by the ECs, while the other 82% are absorbed by the erythrocytes.

In turn, the distribution of $O_2^{\bullet-}$ and H_2O_2 at the ECs' surface in arteries is remarkably similar to that in arterioles (Fig. 3D). This is because the local environment near these vessels' walls is quite similar too, characterized by a slow blood flow, a low hematocrit and important contributions of the ECs for H_2O_2 (and possibly $O_2^{\bullet-}$) clearance. Although deeper into the artery blood flows much faster than in arterioles, few $O_2^{\bullet-}$ and H_2O_2 molecules reach farther than 25 μm from the artery wall (the radius of an arteriole) before dismutating or being absorbed by erythrocytes (Fig. 3E and F). Nevertheless, while the

maximal $O_2^{\bullet-}$ concentration attained near the ECs is quite similar to that attained in arterioles (82% of the latter), that of H_2O_2 is just 44% of that attained in arterioles. This happens because in the artery fewer of the H_2O_2 molecules produced by $O_2^{\bullet-}$ dismutation away from the wall diffuse back. For the same reason, in the artery the H_2O_2 concentration near the ECs reaches its maximum closer to the $O_2^{\bullet-}$-producing region (24 μm from the $O_2^{\bullet-}$ maximum) and shows a slightly steeper decay downstream (50% decay 506 μm downstream from the maximum), despite the faster blood flow.

3.3. Direct H_2O_2 production by the endothelial cells allows mainly short-range signaling

We examined as well the spatial distribution of H_2O_2 along the walls of vessels with the same geometry as above, but where the "active" EC ring releases only H_2O_2 at half the $O_2^{\bullet-}$ release rates considered in the previous simulations (Fig. 4A,D). (That is, the same H_2O_2 production rate as if in the previous simulations all the released $O_2^{\bullet-}$ was dismutated into H_2O_2.) The results for capillaries show that a higher maximal H_2O_2 concentration (11 nM vs. 6.3 nM) is attained in this case (Fig. 4B). This is due to the following two factors. First, there is no $O_2^{\bullet-}$ loss to cellular absorption. Second, H_2O_2 generation is more concentrated in space, as it is not preceded by $O_2^{\bullet-}$ diffusion. The latter factor also implies that the H_2O_2 concentration declines even more steeply along the longitudinal direction, decreasing by 50% over 13. μm and to 1 nM over 34. μm downstream of the maximum. The radial concentration gradient remains negligible (Fig. 4C).

In turn, in arterioles and arteries H_2O_2 concentrations attained at the ECs' surface — 1.6 nM and 1.2 nM, respectively — greatly exceed those attained if ECs release only $O_2^{\bullet-}$ (Fig. 4E,H). However, the concentration decreases very steeply downstream form production zones: in arterioles
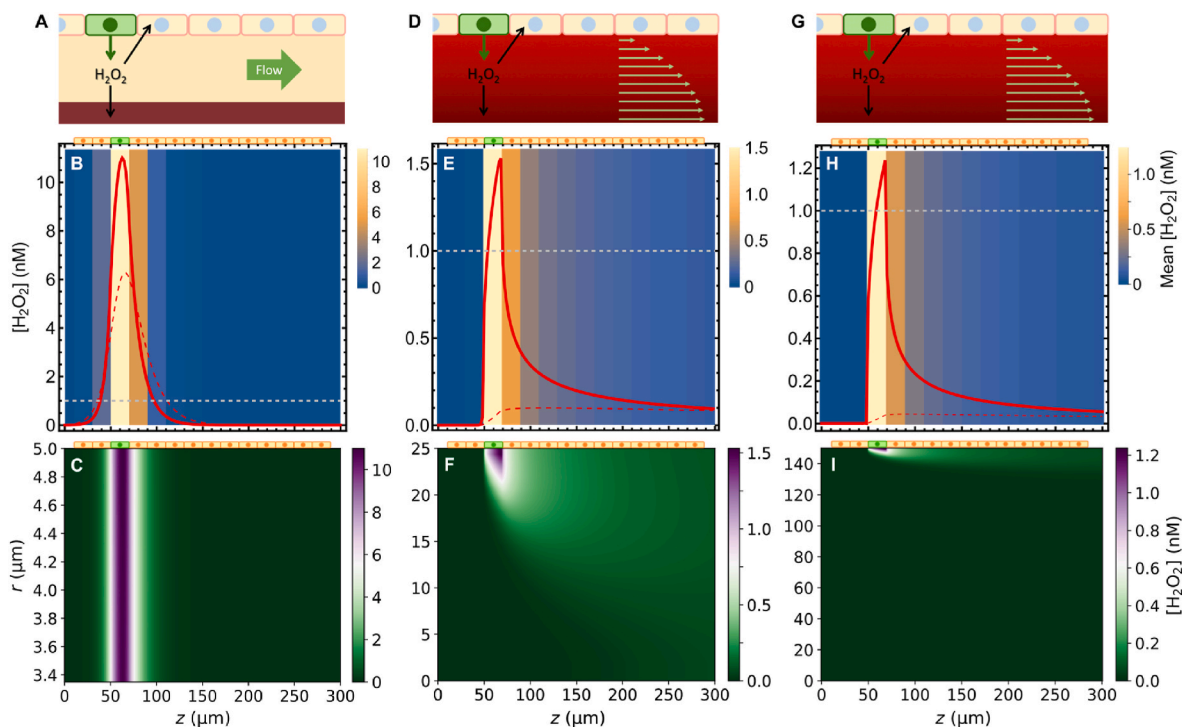
Fig. 4. Spatial distribution of H_2O_2 in capillaries (A–C), arterioles (D–F) and arteries (G–I) where the ECs release only H_2O_2. (A,D,G) Processes considered by the models: H_2O_2 release by the "active" ECs in green, H_2O_2 absorption by all ECs and erythrocytes, H_2O_2 diffusion and advection. (B,E,H) H_2O_2 concentrations at the ECs' surface. The thin dashed red lines show the concentrations for the case where the "active" ECs release only $O_2^{\bullet-}$, for comparison. The background colors represent the average concentration at the surface of each EC represented at the top. The horizontal dashed line marks the assumed signaling threshold. (C,F,I) H_2O_2 concentrations along the radial and longitudinal directions. Note that the r scale is stretched relative to the z scale in these panels. The position of the H_2O_2-producing ECs is marked in green in all panels. Note the distinct length and concentration scales from panel to panel. (For interpretation of the references to color in this figure legend, the reader is referred to the Web version of this article.)

the concentration reaches 1 nM and decreases by 50% from maximal 2.5 μm and 6.0 μm downstream of the maximum, respectively; in arteries these distances are ≤ 2. μm and 4. μm, respectively. Nevertheless, the H_2O_2 distribution shows a heavy downstream tail, due to H_2O_2 molecules that diffuse further into the vessel, are advected there by the faster blood flow, and then diffuse back to the vessel wall. For this reason, the signaling threshold may be exceeded over a much longer range if H_2O_2 release substantially increases. The radial concentration gradient near the production zone is also quite steeper than in the case where the H_2O_2 is produced from $O_2^{\bullet-}$ dismutation in the blood plasma (compare Fig. 4F, I to Fig. 3C,F, respectively).

Again, both the H_2O_2 concentrations and their longitudinal distribution near the walls of arterioles and arteries are remarkably similar.

3.4. Maximal H_2O_2 concentrations attainable in blood plasma are up to the 10 nM range

Figs. 2–4 show that under the reference conditions and production geometry H_2O_2 concentrations at the ECs' surface peak at 6.5 nM, 0.1 nM and 0.44 nM in capillaries, arterioles and arteries, respectively, in the case where ECs release $O_2^{\bullet-}$; and at 11 nM, 1.6 nM and 1.2 nM, in the case where ECs release H_2O_2. As per the model equations, these concentrations are directly proportional the area-specific $O_2^{\bullet-}$ or H_2O_2 release rates, and they increase with the release area. Thus, to better assess the maximal H_2O_2 concentrations attainable, we computed the proportionality constants between concentration at the ECs' surface and area-specific release rate in blood vessels where all ECs release $O_2^{\bullet-}$ or H_2O_2 (Table 2). Considering these proportionality constants, we then computed the H_2O_2 concentrations at the ECs' surface for the reference $O_2^{\bullet-}/H_2O_2$ area-specific supply rates, and for an upper limit corresponding to the most $O_2^{\bullet-}$ productive fully activated phagocytic cells —

Table 2

Proportionality constants between H_2O_2 concentrations at the surface of ECs and area-specific $O_2^{\bullet-}$ or H_2O_2 production rates by the vessel walls for the case of uniform production along the vessels, and H_2O_2 concentrations attained for the reference production rate and for an extreme value.

Vessel	Species released	Proportionality constant (nM/ molecules s^{-1} μm^{-2})	[H_2O_2] for P = 600 $O_2^{\bullet-}$ molecules s^{-1} μm^{-2} (nM)[a]	[H_2O_2] for P = 6×10^4 $O_2^{\bullet-}$ molecules s^{-1} μm^{-2} (nM)[a]
Capillaries	$O_2^{\bullet-}$	2.5×10^{-2}	15	1500
	H_2O_2	5.6×10^{-2}	17	1700
Arterioles	$O_2^{\bullet-}$	7.6×10^{-3}	4.6	460
	H_2O_2	2.0×10^{-2}	6.0	600
Arteries	$O_2^{\bullet-}$	3.7×10^{-3}	2.2	220
	H_2O_2	1.4×10^{-2}	4.2	420

[a] Where ECs are considered to release H_2O_2, the area-specific H_2O_2 production rates considered as reference and upper bound are 300 and 3×10^4 molecules s^{-1} μm^{-2}, respectively.

$\approx 6 \times 10^4$ molecules s^{-1} μm^{-2} [63,64]. We performed these simulations for capillaries, arterioles, and a 150 μm radius small artery. As expected, local H_2O_2 concentrations are slightly higher when ECs release H_2O_2 than when they release $O_2^{\bullet-}$ at twice that rate. But even in the former case, those concentrations do not exceed 17 nM, 6.0 nM and 4.2 nM in capillaries, arterioles and arteries, respectively, for the reference release rates. And even in the implausible upper limit considered, those concentrations would not exceed 1.7 μM, 0.60 μM and 0.42 μM respectively.

These low concentrations are mainly a consequence of the enormous H_2O_2 clearance capacity by erythrocytes and ECs. Because erythrocytes in the arterioles consume 77%–82% of the H_2O_2 when all ECs produce H_2O_2 or $O_2^{\bullet-}$, clearance by erythrocytes alone would suffice to keep H_2O_2 concentrations in the microvasculature lumen sub-μM for plausible

production rates. The reasons for this large clearance capacity are threefold. First, the very high erythrocyte surface area per unit blood volume (630 m^2/L for a 0.45 average hematocrit). Second, the high permeability of erythrocyte membranes to H_2O_2 (Table 1). Third, the large cytosolic H_2O_2 clearance capacity of these cells' cytosol. The catalase activity alone is sufficient to sustain a large transmembrane concentration gradient even should the Prdx and glutathione pools become fully oxidized, meaning that nearly every H_2O_2 entering the cytosol is immediately consumed. Adding to this, •NO released from erythrocytes as a product the strong nitrite reductase activity of hemoglobin [70] may, under some circumstances, help scrub $O_2^{•-}$ from the blood plasma thereby also suppressing H_2O_2 generation.

Remarkably, H_2O_2 concentrations near the walls of larger vessels are in the range of those found for arterioles for similar area-specific $O_2^{•-}$/ H_2O_2 release rates, despite the much lower area/volume ratios of the former vessels (Table 2). This occurs because H_2O_2 clearance is diffusion-limited in the radial length scale of the larger vessels, with characteristic diffusion lengths in the range of the arterioles' radius.

Relevant for potential communication between ECs and erythrocytes, in arterioles where all the ECs produce $O_2^{•-}$ there is a modest radial H_2O_2 concentration gradient: the minimal concentration, at the vessel center, is just 12% lower than the maximal one, attained 2.6 μm from the vessel wall (Fig. S1B). In turn, in arterioles where all the ECs produce H_2O_2, the concentration is maximal adjacent to the vessel's wall and 48% lower at the vessel's center (Fig. S1E). In contrast, in the small artery, the H_2O_2 concentration decreases near-exponentially with the distance from the wall, attaining half-maximal values 23. μm (10. μm) away if all ECs release $O_2^{•-}$ (H_2O_2) (Figs. S1C and F). This behavior and characteristic distances should be similar in larger vessels. $O_2^{•-}$ concentrations at the small artery's center are nearly four orders of magnitude lower, and those of H_2O_2 nearly three orders of magnitude lower, than near the wall. (But note that the model neglects $O_2^{•-}$/H_2O_2 release by plasma enzymes and circulating cells, which may contribute to substantially higher concentrations towards the arteries' center.) Therefore, H_2O_2 eventually produced from a patch of active ECs at one side of even a small artery does not reach the opposite side.
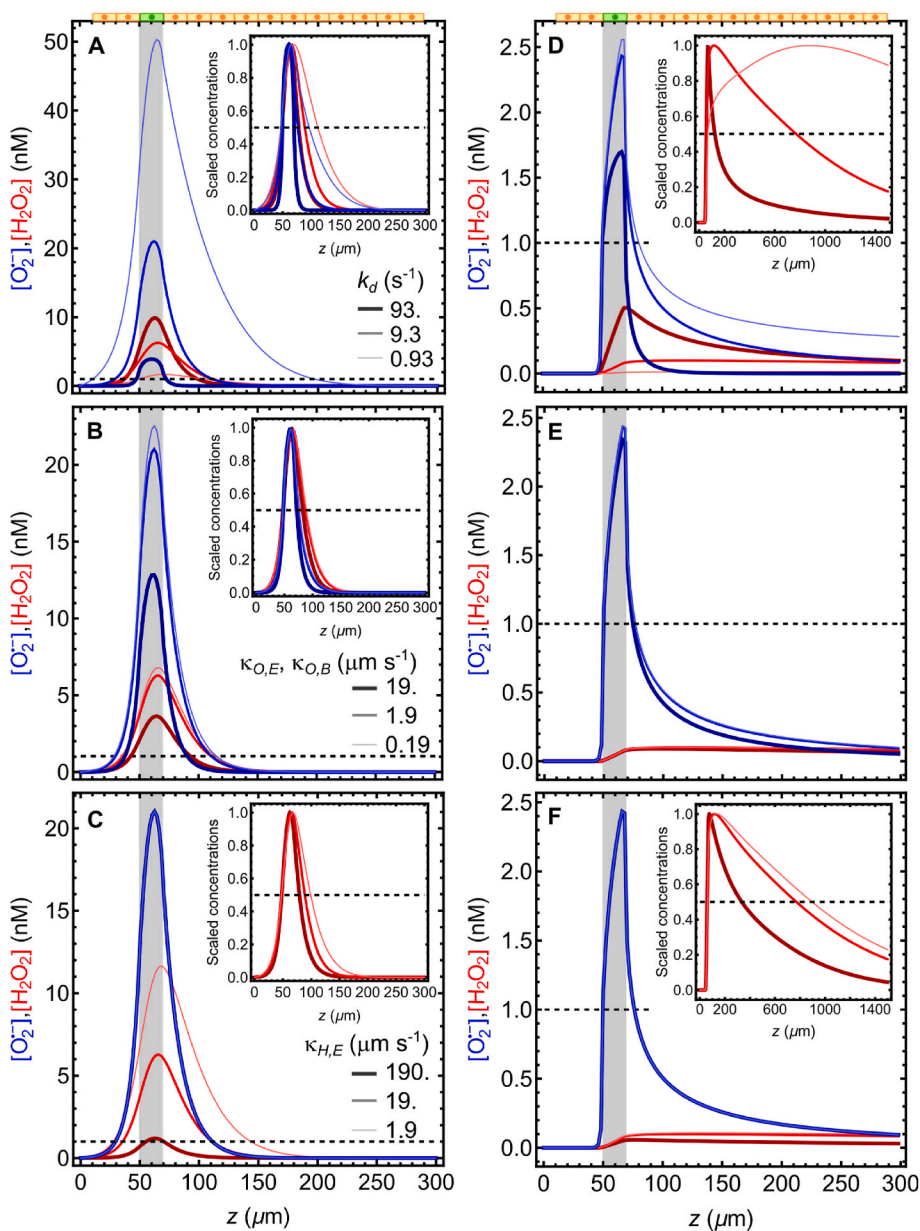
Fig. 5. Main factors influencing H_2O_2 (red) and $O_2^{•-}$ (blue) concentrations at the EC's surface, in capillaries (A–C) and arterioles (D–F) for 10-fold (thick dark lines), 1-fold (medium lines) and 0.1-fold (thin light lines) the reference values of k_d (A, D), $\kappa_{O,B}$ and $\kappa_{O,E}$ together (B, E) and $\kappa_{H,E}$ (C, F). The insets show the concentrations scaled by the respective maxima in each condition. The horizontal dashed lines in the main plots mark the 1 nM H_2O_2 signaling threshold, those in the insets mark the half-maximal concentrations. The gray bars mark the position of the $O_2^{•-}$-producing EC ring. (For interpretation of the references to color in this figure legend, the reader is referred to the Web version of this article.)

3.5. Main factors modulating concentrations and ranges

Besides the production rate, the $O_2^{\bullet-}$ dismutation pseudo-first-order rate constant (k_d) is the parameter with the strongest influence on the maximal $O_2^{\bullet-}$ concentrations near the walls of both microvessels, and it also substantially influences H_2O_2 concentrations at this radial location (Fig. 5A,D). In arterioles, it very strongly influences the H_2O_2 downstream transport range (Fig. 5D inset). Increasing k_d decreases the $O_2^{\bullet-}$ maximal concentrations and the downstream transport range of both chemical species, whereas it increases H_2O_2 concentrations. The substantial variation in H_2O_2 concentration is a consequence of the large sensitivity to k_d of the $O_2^{\bullet-}$ levels in arterioles far from the $O_2^{\bullet-}$ production site. The influence of k_d on $O_2^{\bullet-}$ concentrations at the ECs' surface in the production site is weaker because the steep $O_2^{\bullet-}$ gradients create large $O_2^{\bullet-}$ diffusion fluxes away from this site, such that most $O_2^{\bullet-}$ diffuses away before it dismutates. The opposite occurs in locations of small $O_2^{\bullet-}$ gradients (Fig. 5D).

The permeability constant of EC and erythrocyte membranes to $O_2^{\bullet-}$ is the most uncertain parameter in this model. However, this parameter has very little influence on the $O_2^{\bullet-}$ and H_2O_2 transport ranges in capillaries and arterioles, and on these species' concentrations near arteriole walls (Fig. 5B,E). In capillaries, a 10-fold increase of this permeability constant over its reference value, placing it at the same value as the permeability constant of EC membranes for H_2O_2, substantially decreases the $O_2^{\bullet-}$ and H_2O_2 concentrations, but a 10-fold decrease has very little influence. This is because in the former case, but not in the latter, $O_2^{\bullet-}$ influx into ECs and erythrocytes becomes competitive with dismutation. In arterioles, the permeability constant to $O_2^{\bullet-}$ has an even weaker influence because an even higher fraction of the $O_2^{\bullet-}$ is dismutated.

The permeability constant of EC membranes to H_2O_2 has no effect on the $O_2^{\bullet-}$ concentration or transport ranges. However, it strongly influences the maximal H_2O_2 concentrations at the ECs' surface in capillaries (Fig. 5C), and also substantially influences the H_2O_2 transport range in arterioles at the same radial location (Fig. 5F inset). Increasing $\kappa_{H,E}$ decreases both H_2O_2's maximal concentration and transport range. This happens because for the reference values of the parameters the ECs consume most of the H_2O_2 near these vessels' walls.

Results for arteries should closely mirror those presented above for arterioles.

3.6. Is $O_2^{\bullet-}$ intake a significant H_2O_2 delivery route to the ECs' cytosol?

Under the reference conditions, peak $O_2^{\bullet-}$ concentrations at the ECs' surface substantially exceed H_2O_2's, whether $O_2^{\bullet-}$ release by the vessels' wall is considered localized (insets in Figs. 2A and 3A) or uniform (Figs. S1A,B,C). These results suggest that a substantial fraction of the H_2O_2 supply to the ECs' from $O_2^{\bullet-}$ released to the vessels' lumen might result from cytosolic dismutation of uptaken $O_2^{\bullet-}$. Fig. 6 shows the direct H_2O_2 influx rates into the cytosol and the H_2O_2 generation rates from uptaken $O_2^{\bullet-}$ on the assumption that all of the latter is dismutated, for several values of the $O_2^{\bullet-}$ permeability constants and k_d. In capillaries, $O_2^{\bullet-}$ influx contributes modestly for H_2O_2 supply to the cytosol, for the reference values of the parameters (compare blue to red mid-thickness lines in Fig. 6A). However, it becomes the predominant pathway near the $O_2^{\bullet-}$ production zone if extracellular dismutation becomes slower and/or the permeability of EC and erythrocyte membranes for $O_2^{\bullet-}$ is comparable to that for H_2O_2 (Fig. 6A and B). In arterioles, $O_2^{\bullet-}$ influx supplies most of the H_2O_2 to the cytosol near the $O_2^{\bullet-}$ production zone even for the reference values of the parameters (Fig. 6C, mid-thickness
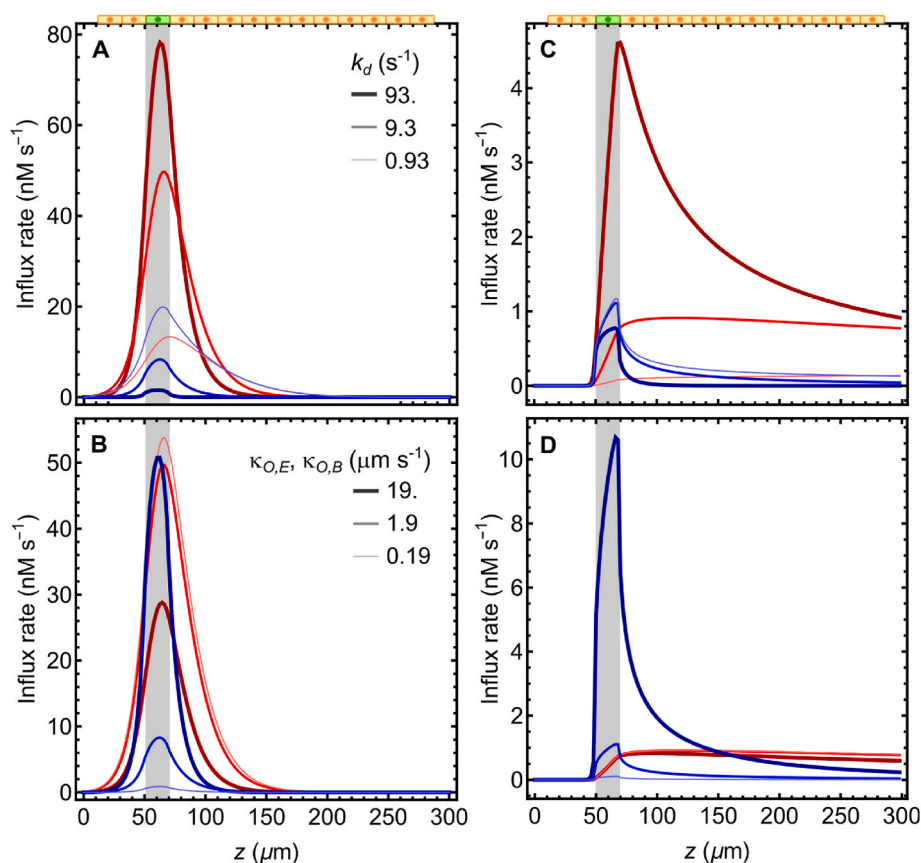
Fig. 6. Hydrogen peroxide supply rate to the cytosol of ECs via direct influx (red) or $O_2^{\bullet-}$ influx followed by dismutation (blue), in capillaries (A,B) and arterioles (C, D) for 10-fold (thick dark lines), 1-fold (medium lines) and 0.1-fold (thin light lines) the reference values of k_d (A, B) and $\kappa_{O,E}$ (C, D). The gray bars mark the position of the $O_2^{\bullet-}$-producing EC ring. (For interpretation of the references to color in this figure legend, the reader is referred to the Web version of this article.)

lines). This becomes true over several tens of μm downstream if extra-cellular dismutation becomes slower and/or the permeability of EC and erythrocyte membranes for $O_2^{\bullet-}$ is comparable to that for H_2O_2 (Fig. 6C and D).

If all the ECs release $O_2^{\bullet-}$, for the reference parameter values, $O_2^{\bullet-}$ influx contributes 11%, 6.8% and 10% of the H_2O_2 supply to the ECs' cytosol in capillaries, arterioles and arteries, respectively. These relative contributions are substantially lower than in the $O_2^{\bullet-}$-producing region in Fig. 6C and D because in the latter case little H_2O_2 reaches this region, due to advection by the blood flow.

4. Discussion

4.1. H_2O_2 concentrations in the vasculature lumen are up to the 10 nM range

Physiological H_2O_2 concentrations in blood plasma have often been claimed to be in the μM range [43 and references therein]. However, the results above (Figs. 2–4, Table 2) show that for plausible $O_2^{\bullet-}$ or H_2O_2 release rates by the EC, the H_2O_2 concentrations attained at the ECs' surface do not exceed 17 nM, 6 nM and 4 nM in capillaries, arterioles and arteries, respectively. Achieving μM H_2O_2 concentrations in micro-vessels would require all the ECs releasing $O_2^{\bullet-}$ to the lumen at the maximal $O_2^{\bullet-}$ production rates achievable by the most productive phagocytic cells when maximally activated, which is very implausible. The following independent experimental evidence further supports physiological H_2O_2 concentrations in blood plasma not exceeding the 10's nM scale. From the permeability constant of the erythrocyte membrane for H_2O_2 (Table 1) one derives a 30. s^{-1} apparent rate constant for H_2O_2 influx into the cytosol (see SI3). In turn, the erythrocyte's capacity to reduce the disulfide form of Prdx2 is limited to 1–2 μM s^{-1} [23,65]. Because Prdx2 reduces most of the H_2O_2 in human erythrocytes [23,65,71], H_2O_2 influx rates in excess of ≈ 2 μM s^{-1} — corresponding to ≈ 80 nM plasma H_2O_2 — should extensively oxidize this protein. However, Prdx2 is modestly oxidized in erythrocytes, even under lipopolysaccharide-induced endotoxemia, which strongly stimulates H_2O_2 production by circulating phagocytes [72,73]. Therefore, H_2O_2 in blood plasma does not reach the 100 nM range systemically. And because $O_2^{\bullet-}$ entering the erythrocyte is dismutated and most of the ONOOH reaching the cytosol also oxidizes Prdx2, the considerations above constrain the total influx of these species into erythrocytes as well. Several studies and critical reviews of *in vitro* experiments determining $O_2^{\bullet-}/H_2O_2$ production and concentrations in the blood further support the conclusion that physiological systemic plasma H_2O_2 concentrations are in the nM range [65,74,75]. Authors claiming otherwise may have underappreciated the H_2O_2 clearance capacity of erythrocytes and ECs *in vivo*, which limits H_2O_2's half-life to <40 ms and thus makes *ex vivo* methods unsuitable for these experimental determinations (see SI2).

The results above do not exclude that H_2O_2 reaches higher concentrations locally and transiently. *E.g.*, wounding may trigger a transient (10-min scale) accumulation of low-μM H_2O_2 concentrations within tens of μm of wound margins [1,7]. However, such H_2O_2 accumulation is driven by DUOX-mediated H_2O_2 production by epithelial cells, not by cells within the vasculature [1]. What the present analysis highlights is the following. Lumenal H_2O_2 concentrations in excess of tens of nM are very unlikely to be reached in normal-functioning vasculature as a consequence of endothelial $O_2^{\bullet-}/H_2O_2$ production, even locally or transiently. Moreover, maximal H_2O_2 concentrations in arterioles and larger vessels should be just up to 35% of those in capillaries for similar $O_2^{\bullet-}$ release rates per μm² of vessel wall (Table 2, Figs. S1C and F).

These conclusions raise the question of how such low H_2O_2 concentration changes can be sensed and transduced. Extracellular H_2O_2 concentrations in the nM scale are still substantially higher than cytosolic ones under physiological conditions [68,69], and therefore cause an influx that can significantly increase cytosolic H_2O_2 concentrations. At such low influx rates — up to 100's nM s^{-1} — virtually all H_2O_2 is captured by cytosolic Prdx1 and Prdx2, which become oxidized and can relay the oxidation to other proteins [27–30]. Given the large Prdx reduction capacities of some human cells [76,77], these low H_2O_2 influx rates may just minimally oxidize the cytosolic Prdx pool. However, scaffold proteins that localize both Prdx and redox targets to the sites of H_2O_2 supply [30] may greatly improve the sensitivity of localized redox relays [12]. Other proposed redox regulation mechanisms appear to be too insensitive for this purpose [12].

Considering the low H_2O_2 influx rates into ECs predicted in this work and H_2O_2's ~0.5 μm diffusion range in the cytosol [12], it is implausible that H_2O_2 from the lumen enters ECs and spreads through gap junctions to promote hyperpolarization of neighboring cells and vasodilation [17].

4.2. Is $O_2^{\bullet-}$ uptake a significant H_2O_2 delivery route to EC?

Estimated $O_2^{\bullet-}$ concentrations at the surface of ECs substantially exceed H_2O_2's (Figs. 2 and 3). They are mainly determined by the dismutation rate constant, and modestly influenced by the permeability of ECs and erythrocytes (Fig. 5). And they raise the question of whether $O_2^{\bullet-}$ influx might contribute substantially for H_2O_2 delivery to ECs. Indeed, even if EC membranes are just 10% as permeable to $O_2^{\bullet-}$ as to H_2O_2, and assuming that all the inflowing $O_2^{\bullet-}$ is dismutated, $O_2^{\bullet-}$ influx supplies most of the H_2O_2 to the cytosol of ECs within the $O_2^{\bullet-}$ production zone of arterioles (Fig. 6C and D). In capillaries, this pathway has a minor contribution to cytosolic H_2O_2 supply under the same conditions, but becomes dominant if ECs' apical membranes are as permeable to $O_2^{\bullet-}$ as to H_2O_2 or if the extracellular SOD activity is substantially lower than the reference values (Fig. 6A and B).

The following experimental observations support the relevance of the $O_2^{\bullet-}$-mediated H_2O_2 delivery route. First, SOD1 inhibition attenuates FGF-2- and VEGF-mediated phosphorylation of ERK1/2 in ECs by preventing the formation of sufficient H_2O_2 to cause inactivation of protein tyrosine phosphatases [78]. Second, SOD1 can drive the specific oxidation of a variety of thiol proteins, presumably through channeling of the H_2O_2 product, and thereby helps adapt cellular metabolism to oxygen availability [79]. Altogether, these computational and experimental results justify paying further attention to the differential responses of vascular ECs to $O_2^{\bullet-}$ *vs*. H_2O_2.

4.3. Potential $O_2^{\bullet-}$ and H_2O_2 signaling through the vasculature can be from autocrine to mm-scale

The simulation results in Figs. 2–4 show that $O_2^{\bullet-}/H_2O_2$ in the (micro)vasculature lumen can signal over widely different ranges. These ranges are shortest for the species ECs directly release, because blood flows very slowly near the vessels' walls and ECs rapidly absorb the H_2O_2 molecules that stay in this region. On the other hand, release of $O_2^{\bullet-}$ by the ECs introduces a delay in H_2O_2 production, which allows this species to reach farther from the signaling cells (Figs. 2A and 3A). In capillaries, this effect just slightly extends the H_2O_2 signaling range because the blood flow is too slow to substantially advect the molecules, transport remaining diffusion dominated (Fig. 2A). In all the situations above, the signaling range is limited to the low 10's of μm, allowing at most communication a few cells across. A very different situation occurs when ECs release $O_2^{\bullet-}$ into the arterioles' and arteries' lumen. Here, there is substantial advection as $O_2^{\bullet-}$ diffuses towards the vessel's center — where blood flows faster — prior to undergoing dismutation, and then the resulting H_2O_2 diffuses back to the vessel's wall. Consequently, H_2O_2 attains maximal concentrations 25–50 μm downstream of the $O_2^{\bullet-}$ concentration maximum, which may allow ECs to signal to downstream cells while minimizing autocrine signaling. Moreover, the H_2O_2 concentration near the ECs decreases longitudinally over a mm scale, thus potentially allowing communication between distant cells. However, this potential long-distance signaling comes at the cost of the maximal H_2O_2 concentrations being very low, such that the considered 1 nM

signaling threshold can only be attained when many cells release $O_2^{\bullet-}$. Therefore, there is a trade-off in H_2O_2 signaling with respect to the mode of H_2O_2 production: direct H_2O_2 release allows attaining higher local concentrations just over a very short range, whereas $O_2^{\bullet-}$ release potentially allows long-range signaling but requires release by a larger number of cells or release at higher rates/cell for H_2O_2 concentrations to attain the signaling threshold. Nevertheless, in arterioles and arteries where H_2O_2 release by the ECs is exacerbated beyond normal levels the signaling range may also extend over many 10's or even 100's of μm. This is because the H_2O_2 distribution near the ECs surface shows a heavy downstream tail, which is due to a minority of H_2O_2 that diffuses some distance away from the vessel wall and then back. But in contrast to what happens in $O_2^{\bullet-}$-mediated H_2O_2 signaling, in this case the producing ECs are exposed to substantially higher H_2O_2 concentrations than any other cells.

At the low concentrations involved in signaling through the vessels' lumen, H_2O_2 entering the ECs will be fully consumed by these cells and will not reach the basal side of the endothelium. However, it may elicit endothelial responses that affect the surrounding tissue.

Besides absorption by ECs, several other factors can affect $O_2^{\bullet-}$ and H_2O_2's reach in the microvasculature lumen. SOD3 activity in the blood plasma is the most prominent of these factors under the reference conditions (Fig. 5). Decreasing SOD3 activity in the blood plasma increases both $O_2^{\bullet-}$'s concentrations and its half-life, thus extending the range of signaling (Fig. 5A,D). In turn, H_2O_2's longitudinal reach in capillaries is mainly determined by the permeability of ECs' apical membranes (Fig. 5C,F). As a consequence, there is a trade-off between signaling sensitivity and spatial range when modulating the permeability of the ECs' membrane to H_2O_2: increasing this permeability enables the ECs to better compete with the erythrocytes for H_2O_2 and increase the rate of H_2O_2 supply to the cytosol, thus further oxidizing Prdx1 and Prdx2 and intensifying signaling; but it also decreases the lifetime and signaling range of extracellular H_2O_2.

4.4. H_2O_2's transport range may vary widely depending on tissue characteristics

How does the transport range of extracellular H_2O_2 in the microvasculature lumen compare to those in "solid" tissues? In the absence of a strong oxidative stress the cytosolic 2-Cys peroxiredoxins sustain a strong transmembrane concentration H_2O_2 gradient [69,80,81]. As a consequence, the clearance rate of extracellular H_2O_2 by the cells is then determined by their membrane's permeability. Thus, at sub-μM extracellular H_2O_2 concentrations, the transport range depends primarily on this permeability and on the volume/area ratio of the extracellular medium. The effective permeability constants inferred from permeation studies of erythrocytes and several human cells in culture are in the 10–20 μm s^{-1} range [22,76]. And a area/volume ratio of $\approx 62. \, \mu m^{-1}$ is inferred from the observation that in the brain cortex — arguably the best characterized tissue in this respect — the extracellular medium accounts for 20% of the tissue volume and has a 60 nm average width [82] (SI4). From these values, one estimates that a H_2O_2 molecule has a <1 ms half-life in the extracellular medium, allowing it to diffuse <3.5 μm on average before being absorbed by a cell. In turn, at extracellular H_2O_2 concentrations in the μM range or higher the cytosolic Prdx pool becomes completely oxidized. As a consequence, the transmembrane H_2O_2 concentration gradient collapses, and the H_2O_2 half-life and transport range increase and become controlled by the activity of the remaining intracellular clearance mechanisms.

How do these theoretical conjectures compare to the few known experimental observations that addressed the transport range of extracellular H_2O_2? In the zebrafish tail wounding model, H_2O_2 concentrations decrease to 50% of maximal values at the wound borders in ≈ 50 μm [7]. In keeping with the conjectures above, these authors observe that the attained H_2O_2 concentrations (5 μM) fully oxidize the peroxiredoxins of the cells within 30 μm of the wound margins, which

decreased H_2O_2 consumption by these cells and broadened the concentration gradient. This phenomenon is very unlikely to occur under non-inflammatory conditions, though.

A recent study of H_2O_2 diffusion and clearance in the brain striatum of living mice determined an effective diffusion coefficient D* = 2.5 × $10^3 \, \mu m^2 \, s^{-1}$ and a 2.2 s half-life, allowing H_2O_2 to diffuse over 180 μm in the extracellular space [10]. These surprisingly long half-life and range may have the following two alternative explanations. First, if the cells in this tissue have permeabilities comparable to those mentioned above, the 1 mM H_2O_2 boluses administered may have fully oxidized the cytosolic peroxiredoxin pool and part of the GSH pool in the measurement field. The modest glutathione peroxidase activity in rat brain tissues [83] would be insufficient to sustain a significant H_2O_2 transmembrane gradient in this case. Therefore, the determined H_2O_2 half-life would then essentially reflect the activity of the remaining intracellular H_2O_2 clearance processes. If this is the correct explanation, the experimental measurement may have strongly overestimated the half-life and transport range that applies at physiological extracellular H_2O_2 concentrations. However, this explanation seems inconsistent with the observation that the first in a series of H_2O_2 boluses administered to the rat brain is already detected by a distant H_2O_2-specific microelectrode with a time course similar to those of subsequent boluses. The inconsistency is because according to the proposed explanation the reactions with the intracellular redox pools would consume the H_2O_2 in the first bolus before it could reach the microelectrode. The alternative explanation is that the long H_2O_2 half-life and transport range are due to most cells in this tissue being virtually impermeable to H_2O_2, perhaps because they are myelinated. In this case, the determined half-life and transport range may be representative of the physiological one for the brain striatum, but does not necessarily apply to other solid tissues. Further research is thus needed to clarify these important issues.

Meanwhile, computational modeling in the vein of the present work will remain an important asset to estimate concentrations and distributions, interpret experimental observations, and designing informative experiments.

5. Concluding remarks

The results in this work show that the blood flow in the vasculature can transport H_2O_2 over a mm-scale, but only when this substance is generated from dismutation of EC-released $O_2^{\bullet-}$ in arterioles and larger vessels. In virtually all the other conditions studied, $O_2^{\bullet-}$ and H_2O_2 transport is limited to <50 μm.

H_2O_2 concentrations in the blood plasma of normal-functioning vasculature do not exceed the low tens of nM, which limits the viable intracellular signal transduction mechanisms

Cellular intake of $O_2^{\bullet-}$ from the blood plasma, followed by cytosolic dismutation, can be a quantitatively significant H_2O_2 signaling route, depending on the plasma SOD activity and on the EC membrane's permeability to $O_2^{\bullet-}$.

Altogether, the theoretical and experimental considerations presented above suggest that H_2O_2's half-life and transport range strongly depend on tissue characteristics. Namely, cell membrane permeability, extracellular space volume/area ratio, intracellular H_2O_2 clearance capacity, mode of extracellular H_2O_2 production and extracellular fluid fluxes.

national funds from FCT – Fundação para a Ciência e a Tecnologia, I.P. through grant SFRH/BD/136046/2018.

Declaration of competing interest

The authors declare that they have no known competing financial interests or personal relationships that could have appeared to influence the work reported in this paper.

Data availability

No data was used for the research described in the article.

Appendix A. Supplementary data

Supplementary data to this article can be found online at https://doi.org/10.1016/j.redox.2022.102527.

References

[1] P. Niethammer, C. Grabher, A.T. Look, T.J. Mitchison, A tissue-scale gradient of hydrogen peroxide mediates rapid wound detection in zebrafish, Nature 459 (2009) 996–999, https://doi.org/10.1038/nature08119.
[2] M.H. Choi, I.K. Lee, G.W. Kim, B.U. Kim, Y.H. Han, D.Y. Yu, H.S. Park, K.Y. Kim, J. S. Lee, C. Choi, Y.S. Bae, B.I. Lee, S.G. Rhee, S.W. Kang, Regulation of PDGF signalling and vascular remodelling by peroxiredoxin II, Nature 435 (2005) 347–353, https://doi.org/10.1038/nature03587.
[3] F. Meda, C. Gauron, C. Rampon, J. Teillon, M. Volovitch, S. Vriz, Nerves control redox levels in mature tissues through schwann cells and hedgehog signaling, Antioxidants Redox Signal. 24 (2016) 299–311, https://doi.org/10.1089/ars.2015.6380.
[4] S. Chatterjee, A.B. Fisher, Mechanotransduction in the endothelium: role of membrane proteins and reactive oxygen species in sensing, transduction, and transmission of the signal with altered blood flow, Antioxidants Redox Signal. 20 (2013) 899–913, https://doi.org/10.1089/ars.2013.5624.
[5] E. Panieri, M.M. Santoro, ROS signaling and redox biology in endothelial cells, Cell. Mol. Life Sci. 72 (2015) 3281–3303, https://doi.org/10.1007/s00018-015-1928-9.
[6] U.E. Martinez-Outschoorn, Z. Lin, C. Trimmer, N. Flomenberg, C. Wang, S. Pavlides, R.G. Pestell, A. Howell, F. Sotgia, M.P. Lisanti, Cancer cells metabolically "fertilize" the tumor microenvironment with hydrogen peroxide, driving the Warburg effect, Cell Cycle 10 (2011) 2504–2520, https://doi.org/10.4161/cc.10.15.16585.
[7] M. Jelcic, B. Enyedi, J.B. Xavier, P. Niethammer, Image-based measurement of H2O2 reaction-diffusion in wounded zebrafish larvae, Biophys. J. 112 (2017) 2011–2018, https://doi.org/10.1016/j.bpj.2017.03.021.
[8] M. Waghray, Z. Cui, J.C. Horowitz, I.M. Subramanian, F.J. Martinez, G.B. Toews, V.J. Thannickal, Hydrogen peroxide is a diffusible paracrine signal for the induction of epithelial cell death by activated myofibroblasts, Faseb. J. 19 (2005) 854–856, https://doi.org/10.1096/fj.04-2882fje.
[9] B. Enyedi, M. Zana, Á. Donkó, M. Geiszt, Spatial and temporal analysis of NADPH oxidase-generated hydrogen peroxide signals by novel fluorescent reporter proteins, Antioxidants Redox Signal. 19 (2012) 523–534, https://doi.org/10.1089/ars.2012.4594.
[10] A. Ledo, E. Fernandes, A. Salvador, J. Laranjinha, R.M. Barbosa, In vivo hydrogen peroxide diffusivity in brain tissue supports volume signaling activity, Redox Biol. 50 (2022), 102250, https://doi.org/10.1016/j.redox.2022.102250.
[11] C.C. Winterbourn, Reconciling the chemistry and biology of reactive oxygen species, Nat. Chem. Biol. 4 (2008) 278–286, https://doi.org/10.1038/nchembio.85.
[12] R.D.M. Travasso, F. Sampaio dos Aidos, A. Bayani, P. Abranches, A. Salvador, Localized redox relays as a privileged mode of cytoplasmic hydrogen peroxide signaling, Redox Biol. 12 (2017) 233–245, https://doi.org/10.1016/j.redox.2017.01.003.
[13] C. Anasooya Shaji, B.D. Robinson, A. Yeager, M.R. Beeram, M.L. Davis, C.L. Isbell, J.H. Huang, B. Tharakan, The tri-phasic role of hydrogen peroxide in blood-brain barrier endothelial cells, Sci. Rep. 9 (2019) 133, https://doi.org/10.1038/s41598-018-36769-3.
[14] R. Alhayaza, E. Haque, C. Karbasiafshar, F.W. Sellke, M.R. Abid, The relationship between reactive oxygen species and endothelial cell metabolism, Front. Chem. 8 (2020), 592688, https://doi.org/10.3389/fchem.2020.592688.
[15] K. Schröder, M. Zhang, S. Benkhoff, A. Mieth, R. Pliquett, J. Kosowski, C. Kruse, P. Luedike, U.R. Michaelis, N. Weissmann, S. Dimmeler, A.M. Shah, R.P. Brandes, Nox4 Is a protective reactive oxygen species generating vascular NADPH oxidase, Circ. Res. 110 (2012) 1217–1225, https://doi.org/10.1161/CIRCRESAHA.112.267054/-/DC1.
[16] R. Bretón-Romero, S. Lamas, Hydrogen peroxide signaling in vascular endothelial cells, Redox Biol. 2 (2014) 529–534, https://doi.org/10.1016/j.redox.2014.02.005.
[17] D.C. Ellinsworth, S.L. Sandow, N. Shukla, Y. Liu, J.Y. Jeremy, D.D. Gutterman, Endothelium-derived hyperpolarization and coronary vasodilation: diverse and integrated roles of epoxyeicosatrienoic acids, hydrogen peroxide, and gap junctions, Microcirculation 23 (2016) 15–32, https://doi.org/10.1111/micc.12255.
[18] G.D. Mao, M.J. Poznansky, Electron spin resonance study on the permeability of superoxide radicals in lipid bilayers and biological membranes, FEBS Lett. 305 (1992) 233–236, https://doi.org/10.1016/0014-5793(92)80675-7.
[19] R.E. Lynch, I. Fridovich, Permeation of the erythrocyte stroma by superoxide radical, J. Biol. Chem. 253 (1978) 4697–4699, https://doi.org/10.1016/s0021-9258(17)30446-5.
[20] B.J. Hawkins, M. Madesh, C.J. Kirkpatrick, A.B. Fisher, Superoxide flux in endothelial cells via the chloride channel-3 mediates intracellular signaling, Mol. Biol. Cell 18 (2007) 2002–2012, https://doi.org/10.1091/mbc.E06–09–0830.
[21] N. Makino, K. Sasaki, K. Hashida, Y. Sakakura, A metabolic model describing the H2O2 elimination by mammalian cells including H2O2 permeation through cytoplasmic and peroxisomal membranes: comparison with experimental data, Biochim. Biophys. Acta - Gen. Subj. 1673 (2004) 149–159, https://doi.org/10.1016/j.bbagen.2004.04.011.
[22] F. Orrico, A.C. Lopez, D. Saliwonczyk, C. Acosta, I. Rodriguez-Grecco, I. Mouro-Chanteloup, M.A. Ostuni, A. Denicola, L. Thomson, M.N. Möller, The permeability of human red blood cell membranes to hydrogen peroxide is independent of aquaporins, J. Biol. Chem. (2021), 101503, https://doi.org/10.1016/j.jbc.2021.101503.
[23] F.M. Low, M.B. Hampton, A.V. Peskin, C.C. Winterbourn, Peroxiredoxin 2 functions as a noncatalytic scavenger of low-level hydrogen peroxide in the erythrocyte, Blood 109 (2007) 2611–2617, https://doi.org/10.1182/blood-2006-09-048728.
[24] L.A.C. Carvalho, D.R. Truzzi, T.S. Fallani, S.V Alves, J.C. Toledo Junior, O. Augusto, L.E.S. Netto, F.C. Meotti, Urate hydroperoxide oxidizes human peroxiredoxin 1 and peroxiredoxin 2, J. Biol. Chem. 292 (2017) 8705–8715, https://doi.org/10.1074/jbc.M116.767657.
[25] B. Manta, M. Hugo, C. Ortiz, G. Ferrer-Sueta, M. Trujillo, A. Denicola, The peroxidase and peroxynitrite reductase activity of human erythrocyte peroxiredoxin 2, Arch. Biochem. Biophys. 484 (2009) 146–154, https://doi.org/10.1016/j.abb.2008.11.017.
[26] S. Portillo-Ledesma, L.M. Randall, D. Parsonage, J.D. Rizza, P.A. Karplus, L. B. Poole, A. Denicola, G. Ferrer-Sueta, Differential kinetics of two-cysteine peroxiredoxin disulfide formation reveal a novel model for peroxide sensing, Biochemistry 57 (2018) 3416–3424, https://doi.org/10.1021/acs.biochem.8b00188.
[27] M.C. Sobotta, W. Liou, S. Stöcker, D. Talwar, M. Oehler, T. Ruppert, A.N. Scharf, T. P. Dick, Peroxiredoxin-2 and STAT3 form a redox relay for H2O2 signaling, Nat. Chem. Biol. 11 (2014) 64–70, https://doi.org/10.1038/nchembio.1695.
[28] T.N. Vo, J.M. Pueyo, K. Wahni, D. Ezerin, J. Bolduc, J. Messens, Prdx1 interacts with ASK1 upon exposure to H2O2 and independently of a scaffolding protein, Antioxidants 10 (2021) 1060, https://doi.org/10.3390/antiox10071060.
[29] R.M. Jarvis, S.M. Hughes, E.C. Ledgerwood, Peroxiredoxin 1 functions as a signal peroxidase to receive, transduce, and transmit peroxide signals in mammalian cells, Free Radic. Biol. Med. 53 (2012) 1522–1530, https://doi.org/10.1016/j.freeradbiomed.2012.08.001.
[30] D. Talwar, J. Messens, T.P. Dick, A role for annexin A2 in scaffolding the peroxiredoxin 2–STAT3 redox relay complex, Nat. Commun. 11 (2020) 1–11, https://doi.org/10.1038/s41467-020-18324-9.
[31] R. Kissner, T. Nauser, P. Bugnon, P.G. Lye, W.H. Koppenol, Formation and properties of peroxynitrite as studied by laser flash photolysis, high-pressure stopped-flow technique, pulse radiolysis, Chem. Res. Toxicol. 10 (1997) 1285–1292, https://doi.org/10.1021/tx970160x.
[32] S.V. Lymar, J.K. Hurst, Rapid reaction between peroxonitrite ion and carbon dioxide: implications for biological activity, J. Am. Chem. Soc. 117 (1995) 8867–8868, https://doi.org/10.1021/JA00139A027.
[33] Y. Neishi, S. Mochizuki, T. Miyasaka, T. Kawamoto, T. Kume, R. Sukmawan, M. Tsukiji, Y. Ogasawara, F. Kajiya, T. Akasaka, K. Yoshida, M. Goto, Evaluation of bioavailability of nitric oxide in coronary circulation by direct measurement of plasma nitric oxide concentration, Proc. Natl. Acad. Sci. U. S. A. 102 (2005) 11456–11461, https://doi.org/10.1073/pnas.0501392102.
[34] N.V. Blough, O.C. Zafiriou, Reaction of superoxide with nitric oxide to form peroxonitrite in alkaline aqueous solution, Inorg. Chem. 24 (1985) 3502–3504, https://doi.org/10.1021/ic00216a003.
[35] S.S. Marla, J. Lee, J.T. Groves, Peroxynitrite rapidly permeates phospholipid membranes, Proc. Natl. Acad. Sci. U. S. A. 94 (1997) 14243–14248, https://doi.org/10.1073/pnas.94.26.14243.
[36] M. Soszynski, G. Bartosz, Penetration of erythrocyte membrane by peroxynitrite: participation of the anion exchange protein, IUBMB Life 43 (1997) 319–325, https://doi.org/10.1080/15216549700204101.
[37] A. Denicola, J.M. Souza, R. Radi, Diffusion of peroxynitrite across erythrocyte membranes, Proc. Natl. Acad. Sci. U. S. A. 95 (1998) 3566–3571, https://doi.org/10.1073/pnas.95.7.3566.
[38] J. Dalla Rizza, L.M. Randall, J. Santos, G. Ferrer-Sueta, A. Denicola, Differential parameters between cytosolic 2-Cys peroxiredoxins, PRDX1 and PRDX2, Protein Sci. 28 (2019) 191–201, https://doi.org/10.1002/pro.3520.
[39] A. Denicola, B.A. Freeman, M. Trujillo, R. Radi, Peroxynitrite reaction with carbon dioxide/bicarbonate: kinetics and influence on peroxynitrite-mediated oxidations,

Arch. Biochem. Biophys. 333 (1996) 49–58, https://doi.org/10.1006/abbi.1996.0363.

[40] J.D. Van Buul, M. Fernandez-Borja, E.C. Anthony, P.L. Hordijk, Expression and localization of NOX2 and NOX4 in primary human endothelial cells, antioxid, Redox Signal 7 (2005) 308–317, https://doi.org/10.1089/ars.2005.7.308.

[41] Y. Nisimoto, B.A. Diebold, D. Cosentino-Gomes, J.D. Lambeth, Nox4: a hydrogen peroxide-generating oxygen sensor, Biochemistry 53 (2014) 5111–5120, https://doi.org/10.1021/BI500331Y.

[42] N.M. Tsoukias, M. Kavdia, A.S. Popel, A theoretical model of nitric oxide transport in arterioles: frequency- vs. amplitude-dependent control of cGMP formation, Am. J. Physiol. Heart Circ. Physiol. 286 (2004) H1043–H1056, https://doi.org/10.1152/ajpheart.00525.2003.

[43] K.M. Smith, L.C. Moore, H.E. Layton, Advective transport of nitric oxide in a mathematical model of the afferent arteriole, Am. J. Physiol. Physiol. 284 (2003) F1080–F1096, https://doi.org/10.1152/ajprenal.00141.2002.

[44] M.W. Vaughn, L. Kuo, J.C. Liao, Effective diffusion distance of nitric oxide in the microcirculation, Am. J. Physiol. Cell Physiol. 274 (1998) H1705–H1714, https://doi.org/10.1152/ajpheart.1998.274.5.H1705.

[45] S. Kar, M. Kavdia, Endothelial NO and O2·⁻ production rates differentially regulate oxidative, nitroxidative, and nitrosative stress in the microcirculation, Free Radic. Biol. Med. 63 (2013) 161–174, https://doi.org/10.1016/j.freeradbiomed.2013.04.024.

[46] X. Liu, P. Srinivasan, E. Collard, P. Grajdeanu, J.L. Zweier, A. Friedman, Nitric oxide diffusion rate is reduced in the aortic wall, Biophys. J. 94 (2008), https://doi.org/10.1529/biophysj.107.120626, 1880–9.

[47] N.M. Tsoukias, Nitric oxide bioavailability in the microcirculation: insights from mathematical models, Microcirculation 15 (2008) 813–834, https://doi.org/10.1080/10739680802010070.

[48] Y. Liu, D.G. Buerk, K.A. Barbee, D. Jaron, A dynamic computational network model for the role of nitric oxide and the myogenic response in microvascular flow regulation, Microcirculation 25 (2018), e12465, https://doi.org/10.1111/micc.12465.

[49] P. Han, D.M. Bartels, Temperature dependence of oxygen diffusion in H2O and D2O, J. Phys. Chem. 100 (1996) 5597–5602, https://doi.org/10.1021/jp952903y.

[50] S.A.M. van Stroe-Biezen, F.M. Everaerts, L.J.J. Janssen, R.A. Tacken, Diffusion coefficients of oxygen, hydrogen peroxide and glucose in a hydrogel, Anal. Chim. Acta 273 (1993) 553–560, https://doi.org/10.1016/0003-2670(93)80202-V.

[51] S.L. Marklund, Extracellular superoxide dismutase and other superoxide dismutase isoenzymes in tissues from nine mammalian species, Biochem. J. 222 (1984) 649–655, https://doi.org/10.1042/bj2220649.

[52] E. Evans, Y.-C. Fung, Improved measurements of the erythrocyte geometry, Microvasc. Res. 4 (1972) 335–347, https://doi.org/10.1016/0026-2862(72)90069-6.

[53] H.H. Billett, Hemoglobin and hematocrit, in: H.K. Walker, W.D. Hall, J.W. Hurst (Eds.), Clin. Methods Hist. Phys. Lab. Exam., third ed., Butterworths, Boston, MA, 1990. https://www.ncbi.nlm.nih.gov/books/NBK259/.

[54] J. West, Best and Taylor's Physiological Basis of Medical Practice, eleventh ed., Williams & Wilkins, Baltimore, Maryland, 1985.

[55] A.R. Pries, T.W. Secomb, Blood flow in microvascular networks, in: R.F. Tuma, W.N. Durán, K. Ley (Eds.), Handb. Physiol. Microcirc., second ed., Academic Press, San Diego, 2008.

[56] H.L. Goldsmith, V.T. Turitto, Rheological aspects of thrombosis and haemostasis: basic principles and applications. ICTH-Report–Subcommittee on Rheology of the International Committee on Thrombosis and Haemostasis, Thromb. Haemostasis 55 (1986) 415–435, https://doi.org/10.1055/S-0038-1661576/ID/JR_17.

[57] R.A. Freitas Jr., Arteriovenous macrocirculation, in: Nanomedicine, Landes Bioscience, Georgetown (TX), 1999.

[58] E. Doutel, F.J. Galindo-Rosales, L. Campo-Deaño, Hemodynamics challenges for the navigation of medical microbots for the treatment of CVDs, Materials 14 (2021) 7402, https://doi.org/10.3390/ma14237402.

[59] R. Fåhræus, T. Lindqvist, The viscosity of the blood in narrow capillary tubes, Am. J. Physiol. Content. 96 (1931) 562–568.

[60] V.L. Kinnula, A.R. Whorton, L.-Y. Chang, J.D. Crapo, Regulation of hydrogen peroxide generation in cultured endothelial cells, Am. J. Respir. Cell Mol. Biol. 6 (1992) 175–182, https://doi.org/10.1165/AJRCMB/6.2.175.

[61] V.L. Kinnula, Z. Mirza, J.D. Crapo, A.R. Whorton, Modulation of hydrogen peroxide release from vascular endothelial cells by oxygen, Am. J. Respir. Cell Mol. Biol. 9 (1993) 603–609.

[62] C. Privat, O. Stepien, M. David-Dufilho, A. Brunet, F. Bedioui, P. Marche, J. Devynck, M.A. Devynck, Superoxide release from interleukin-1β-stimulated human vascular cells: in situ electrochemical measurement, Free Radic. Biol. Med. 27 (1999) 554–559, https://doi.org/10.1016/S0891-5849(99)00097-0.

[63] X.P. Liu, J.L. Zweier, A real-time electrochemical technique for measurement of cellular hydrogen peroxide generation and consumption: evaluation in human polymorphonuclear leukocytes, Free Radic. Biol. Med. 31 (2001) 894–901.

[64] H. Jaeschke, A.P. Bautista, Z. Spolarics, J.J. Spitzer, Superoxide generation by neutrophils and Kupffer cells during in vivo reperfusion after hepatic ischemia in rats, J. Leukoc. Biol. 52 (1992) 377–382, https://doi.org/10.1002/jlb.52.4.377.

[65] R. Benfeitas, G. Selvaggio, F. Antunes, P.M.B.M. Coelho, A. Salvador, Hydrogen peroxide metabolism and sensing in human erythrocytes: a validated kinetic model and reappraisal of the role of peroxiredoxin II, Free Radic. Biol. Med. 74 (2014) 35–49, https://doi.org/10.1016/j.freeradbiomed.2014.06.007.

[66] L.E. Netto, F. Antunes, The roles of peroxiredoxin and thioredoxin in hydrogen peroxide sensing and in signal transduction, Mol. Cells. 39 (2016) 65–71, https://doi.org/10.14348/molcells.2016.2349.

[67] Z.A. Wood, Peroxiredoxin evolution and the regulation of hydrogen peroxide signaling, Science 300 (2003) 650–653, https://doi.org/10.1126/science.1080405 (80).

[68] J.B. Lim, B.K. Huang, W.M. Deen, H.D. Sikes, Analysis of the lifetime and spatial localization of Hydrogen peroxide generated in the cytosol using a reduced kinetic model, Free Radic. Biol. Med. 89 (2015) 47–53, https://doi.org/10.1016/j.freeradbiomed.2015.07.009.

[69] O. Lyublinskaya, F. Antunes, Measuring intracellular concentration of hydrogen peroxide with the use of genetically encoded H2O2 biosensor HyPer, Redox Biol. 24 (2019), 101200, https://doi.org/10.1016/J.REDOX.2019.101200.

[70] M.T. Gladwin, D.B. Kim-Shapiro, The functional nitrite reductase activity of the heme-globins, Blood 112 (2008) 2636–2647, https://doi.org/10.1182/BLOOD-2008-01-115261.

[71] F. Orrico, M.N. Möller, A. Cassina, A. Denicola, L. Thomson, Kinetic and stoichiometric constraints determine the pathway of H2O2 consumption by red blood cells, Free Radic. Biol. Med. 121 (2018) 231–239, https://doi.org/10.1016/j.freeradbiomed.2018.05.006.

[72] S.B. Bayer, G. Maghzal, R. Stocker, M.B. Hampton, C.C. Winterbourn, Neutrophil-mediated oxidation of erythrocyte peroxiredoxin 2 as a potential marker of oxidative stress in inflammation, Faseb. J. 27 (2013) 3315–3322, https://doi.org/10.1096/fj.13-227298.

[73] R.F. Queiroz, C.P. Stanley, K. Wolhuter, S.M.Y. Kong, R. Rajivan, N. McKinnon, G.T.H. Nguyen, A. Roveri, S. Guttzeit, P. Eaton, W.A. Donald, F. Ursini, C.C. Winterbourn, A. Ayer, R. Stocker, Hydrogen peroxide signaling via its transformation to a stereospecific alkyl hydroperoxide that escapes reductive inactivation, 2021, Nat. Commun. 121 (12) (2021) 1–17, https://doi.org/10.1038/s41467-021-26991-5.

[74] B. Frei, Y. Yamamoto, D. Niclas, B.N. Ames, Evaluation of an isoluminol chemiluminescence assay for the detection of hydroperoxides in human blood plasma, Anal. Biochem. 175 (1988) 120–130, https://doi.org/10.1016/0003-2697(88)90369-7.

[75] A. Nahum, L.D.H. Wood, J. Iasha Sznajder, Measurement of hydrogen peroxide in plasma and blood, Free Radic. Biol. Med. 6 (1989) 479–484, https://doi.org/10.1016/0891-5849(89)90040-3.

[76] G. Selvaggio, P.M.B.M. Coelho, A. Salvador, Mapping the phenotypic repertoire of the cytoplasmic 2-Cys peroxiredoxin – thioredoxin system. 1. Understanding commonalities and differences among cell types, Redox Biol. 15 (2018) 297–315, https://doi.org/10.1016/j.redox.2017.12.008.

[77] S. Miller, S.W. Walker, J.R. Arthur, F. Nicol, K. Pickard, M.H. Lewin, A.F. Howie, G.J. Beckett, Selenite protects human endothelial cells from oxidative damage and induces thioredoxin reductase, Clin. Sci. 100 (2001) 543–550, https://doi.org/10.1042/CS1000543.

[78] J.C. Juarez, M. Manuia, M.E. Burnett, O. Betancourt, B. Boivin, D.E. Shaw, N.K. Tonks, A.P. Mazar, F. Doñate, Superoxide dismutase 1 (SOD1) is essential for H2O2-mediated oxidation and inactivation of phosphatases in growth factor signaling, Proc. Natl. Acad. Sci. USA 105 (2008) 7147–7152, https://doi.org/10.1073/PNAS.0709451105.

[79] C. Montllor-Albalate, H. Kim, A.E. Thompson, A.P. Jonke, M.P. Torres, A.R. Reddi, Sod1 integrates oxygen availability to redox regulate NADPH production and the thiol redoxome, Proc. Natl. Acad. Sci. USA 119 (2022), https://doi.org/10.1073/pnas.2023328119.

[80] B.K. Huang, H.D. Sikes, Quantifying intracellular hydrogen peroxide perturbations in terms of concentration, Redox Biol. 2 (2014) 955–962, https://doi.org/10.1016/j.redox.2014.08.001.

[81] A. Domènech, J. Ayté, F. Antunes, E. Hidalgo, Using in vivo oxidation status of one- and two-component redox relays to determine H2O2 levels linked to signaling and toxicity, BMC Biol. 16 (2018) 61, https://doi.org/10.1186/s12915-018-0523-6.

[82] E. Syková, C. Nicholson, Diffusion in brain extracellular space, Physiol. Rev. 88 (2008) 1277–1340, https://doi.org/10.1152/physrev.00027.2007.

[83] X. Sun, A.Y. Shih, H.C. Johannssen, H. Erb, P. Li, T.H. Murphy, Two-photon imaging of glutathione levels in intact brain indicates enhanced redox buffering in developing neurons and cells at the cerebrospinal fluid and blood-brain interface, J. Biol. Chem. 281 (2006) 17420–17431, https://doi.org/10.1074/jbc.M601567200.